

Reduced Reference Perceptual Quality Model and Application to Rate Control for 3D Point Cloud Compression

Qi Liu, Hui Yuan, *Senior Member, IEEE*, Raouf Hamzaoui, *Senior Member, IEEE*,
Honglei Su, Junhui Hou, *Senior Member, IEEE*, and Huan Yang, *Member, IEEE*

Abstract—In rate-distortion optimization, the encoder settings are determined by maximizing a reconstruction quality measure subject to a constraint on the bit rate. One of the main challenges of this approach is to define a quality measure that can be computed with low computational cost and which correlates well with perceptual quality. While several quality measures that fulfil these two criteria have been developed for images and video, no such one exists for 3D point clouds. We address this limitation for the video-based point cloud compression (V-PCC) standard by proposing a linear perceptual quality model whose variables are the V-PCC geometry and color quantization parameters and whose coefficients can easily be computed from two features extracted from the original 3D point cloud. Subjective quality tests with 400 compressed 3D point clouds show that the proposed model correlates well with the mean opinion score, outperforming state-of-the-art full reference objective measures in terms of Spearman rank-order and Pearson's linear correlation coefficient. Moreover, we show that for the same target bit rate, rate-distortion optimization based on the proposed model offers higher perceptual quality than rate-distortion optimization based on exhaustive search with a point-to-point objective quality metric.

Index Terms—Point cloud, perceptual quality metric, subjective test, content features, rate-distortion optimization (RDO).

I. INTRODUCTION

WITH the rapid development of 3D data acquisition technologies, point clouds are now readily available and popular. A 3D point cloud (3DPC) comprises a set of points with geometric coordinates and associated attributes, such as color, reflectance, normal vectors, and so on. These points can be stored, transmitted, and rendered in a variety of ways. There

are already many 3DPC applications in the fields of virtual reality, immersive communication, architecture, and automatic driving, etc. [1]. 3DPCs can be classified into objects and scenes. Each class can consist of static or dynamic 3DPCs. In this paper, we mainly focus on static 3DPC objects [2].

To represent the surface of an object with high fidelity, a 3DPC usually contains millions, even billions of points, which results in a large amount of data that needs to be efficiently stored and transmitted [3]. Recently, the Moving Picture Experts Group (MPEG) standardized two compression platforms for Point Cloud Compression (PCC): Geometry-based Point Cloud Compression (G-PCC) [4] and Video-based Point Cloud Compression (V-PCC) [5]. In these platforms, both geometry and color information are compressed [6]. Therefore, the distortion of geometry and color will inevitably influence the perceived quality of the reconstructed 3DPCs.

Similar to image/video quality assessment methods, point cloud quality assessment methods can be classified into three categories: Full Reference (FR), Reduced Reference (RR), and No Reference (NR). To evaluate the quality of a distorted point cloud, FR methods use the pristine uncompressed point cloud as a reference, while RR methods only require statistical features that are extracted from the reference point cloud. On the other hand, NR methods evaluate the quality of the distorted point cloud in the absence of the reference one.

FR 3DPC objective quality assessment techniques can be based on the point-to-point [7], point-to-plane [8] or point-to-mesh [9] distortion metric. The point-to-point metric uses geometric distances between points in the reference and distorted 3DPC, but it does not consider the fact that points in a 3DPC usually represent surfaces on the object. The point-to-plane metric is based on the projected error along the normal of a reference point. This method depends on the calculation of the normal and, essentially, larger costs are assigned to points deviated from the underlying surface. The point-to-mesh [9] metric requires construction of 3D meshes and is therefore hard to deploy in real time applications. Beyond that, there is an angular similarity-based FR metric [10] and a local curvature analysis-based FR metric [11] for 3DPC quality assessment. Both of them are limited by the high complexity of searching for the neighboring points to construct the normal or curvature. In addition, the above objective quality metrics cannot predict the visual quality of 3DPCs accurately, especially when the coding distortion is involved [12] [13].

In this paper, we propose a reduced reference model to

This work was supported in part by the National Natural Science Foundation of China under Grant 61871342; in part by the open project program of state key laboratory of virtual reality technology and systems, Beihang University, under Grant VRLAB2019B03; in part by the Hong Kong Research Grants Council under Grants 9042955 (CityU 11202320), and in part by Shandong Provincial Natural Science Foundation, China under Grants ZR2018PF002. Corresponding author: Hui Yuan.

Q. Liu is with the School of Information Science and Engineering, Shandong University, Qingdao 266237, China. (Email: sdqi.liu@gmail.com).

H. Yuan is with the School of Control Science and Engineering, Shandong University, Ji'nan 250061, China. (Email: huiyuan@sdu.edu.cn).

R. Hamzaoui is with the School of Engineering and Sustainable Development, De Montfort University, Leicester, UK. (Email: rhamzaoui@dmu.ac.uk).

H. Su is with the School of Electronic Information, Qingdao University, Qingdao 266071, China. (Email: suhonglei@qdu.edu.cn).

J. Hou is with the Department of Computer Science, City University of Hong Kong, Kowloon, Hong Kong. (Email: jh.hou@cityu.edu.hk).

H. Yang is with the College of Computer Science and Technology, Qingdao University, Qingdao 266071, China. (Email: cathy_huanyang@hotmail.com).

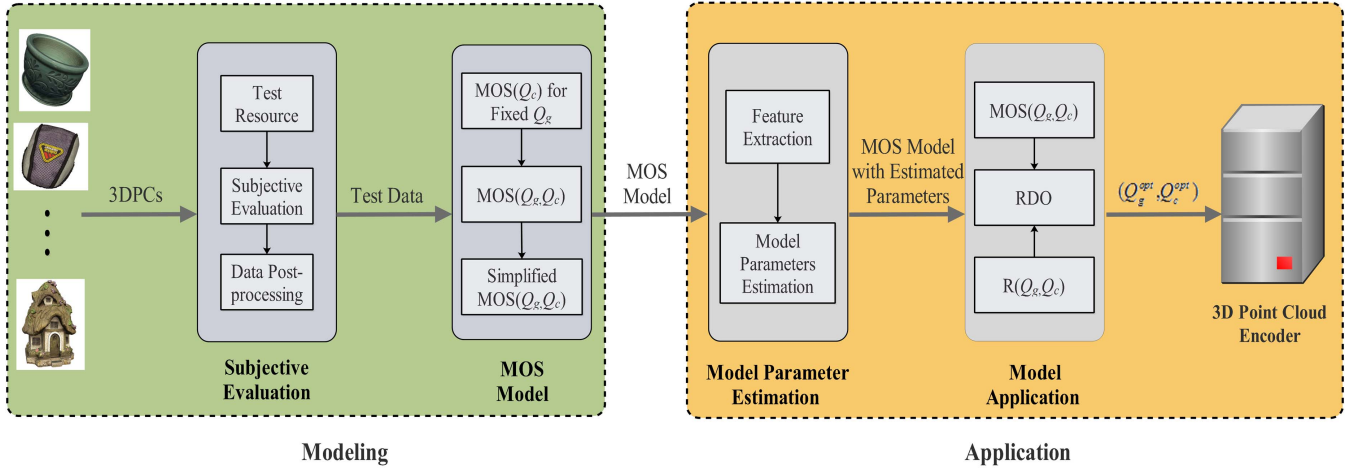


Fig. 1. Compressed 3DPC perceptual quality modeling and its application. Q_g and Q_c denote the geometry quantization step and color quantization step, respectively, (Q_g^{opt}, Q_c^{opt}) is the optimal geometry and color quantization step pair, $R(\cdot)$ and $MOS(\cdot)$ are the rate and MOS functions, respectively.

accurately predict the mean opinion score (MOS) of V-PCC compressed 3DPCs from the quantization parameters of the geometry and color encoders. The proposed model is analytically simple and can be used for rate-distortion optimized (RDO) rate control, as shown in Fig. 1. The main contributions of this paper are as follows:

- 1) We conduct comprehensive subjective tests to obtain MOSs of V-PCC compressed 3DPCs with different combinations of geometry and color quantization steps.
- 2) We develop a simple yet effective analytical model to predict the MOS from the geometry and color quantization steps.
- 3) We study the dependent factors of the model parameters and propose two features to estimate them.
- 4) We propose a perceptually optimal rate control method based on the proposed analytical model.

The remainder of this paper is organized as follows. Section II briefly reviews related work. The subjective test and the test results are described in Section III. In Section IV, we present the proposed perceptual quality model and validate its accuracy by using the subjective test results. The dependent factors of the model parameters are studied in Section V. Based on the study, we propose an efficient model parameter estimation method by extracting two features from the original 3DPCs. Subsequently, the subjective quality-based rate control method is presented and evaluated in Section VI. Finally, Section VII concludes the paper.

II. RELATED WORK

To develop an accurate perceptual quality model for 3DPCs, subjective experiments are necessary. In recent years, some datasets were provided to study the impact of compression on the subjective quality of the reconstructed point clouds. Alexiou *et al.* [14] provided a database which has eight reference point clouds and the tested point clouds are compressed by G-PCC and V-PCC. Zerman *et al.* [15] used V-PCC to generate a dataset of 3DPCs showing two people playing football. The remaining datasets [16] [17] study the impact of multiple

degradations types on point cloud subjective quality, without focusing on the compression degradation type. Usually, the number of raw 3DPCs limits the accuracy of the subjective quality test. Therefore, we need to build a new subjective test dataset that contains sufficient reference content and various encoding degradation levels.

Generally, subjective quality assessment tests involve the participation of subjects in experiments in which distorted objects are visualized and rated. In [13], [18], [19], the geometry distortion was evaluated, while the effect of color distortion was ignored. Torlig *et al.* [20] considered the geometry and color distortion jointly when doing the subjective assessment. However, only six 3DPCs and their related degradations were assessed. Su *et al.* [21] proposed a complete point cloud data sets with various quality levels and made preliminary verification on the performance of the existing objective quality evaluation model. As reported in [21], the visual information fidelity in pixel domain (VIFP) achieves the best performance compared to other assessment models. However, the PLCC and SRCC of VIFP is only 0.77 which means the accuracy of 3DPC quality assessment model still needs to be improved. Inspired by the human visual system (HVS), eyes are not directly sensing the individual point intensity, but rather the connected local neighbor structures due to the low-pass spread functionality of our eye optics [22]. Yang *et al.* [23] proposed a graph-based objective metric instead of a point-based one. Although the metric can predict the MOS more accurately than point-wise metrics, the resampling and local graph construction operations greatly increase its complexity, which limits its applications. Moreover, the existing FR objective 3DPC quality model is hard to be satisfied in some applications. For example, in 3DPC streaming, a 3DPC is often requested by users with diverse sustainable channel bandwidth. To address this diversity, it can be coded into a scalable stream with several geometry and color quantization parameters (QPs) combinations. Given a particular target bitrate, the encoder needs to determine appropriate geometry and color QPs to achieve the best perceptual quality. When there are only

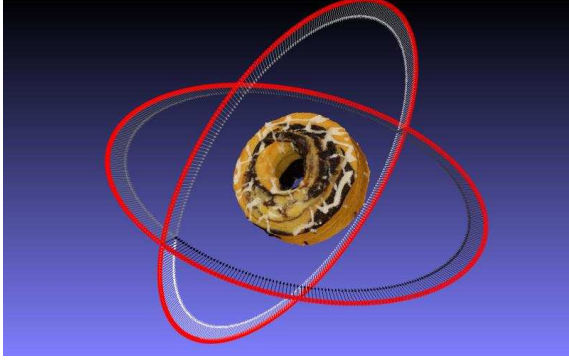


Fig. 2. Illustration of the generation of pictures from 360 viewpoints of a 3DPC.

FR metrics, time consuming exhaustive pre-coding must be conducted to evaluate the performance of different QP combinations [24] [25] [26]. In [24], a model-based technique was developed to efficiently determine the optimal maximum octree level (geometric distortion) and JPEG_VALUE (color distortion) for point cloud library-based point cloud compression (PCL-PCC) platform. However, only the color difference between the original point cloud and the reconstructed point cloud was considered in the bit allocation problem. In [25], a linear combination of the geometry and color distortions was used to represent the point-to-point distortion of 3DPCs. In [26], a coarse to fine rate control algorithm was proposed, in which the point-to-point distortion metric was also adopted. In all those methods, the perceptual quality of the reconstructed 3DPCs was not considered, which may limit their performance to some extent.

III. SUBJECTIVE QUALITY ASSESSMENT

A. Subjective test dataset

It is hard for an observer to distinguish the quality degradation of 3DPC with intrinsic distortion [18]. In the early stage of the MPEG standardization for point cloud compression (PCC), there are not enough high quality raw 3DPCs. Therefore, sixteen high quality point clouds, i.e., *Bag* (1267845 points), *Banana* (807184 points), *Biscuits* (952579 points), *Cake* (2486566 points), *Cauliflower* (1936627 points), *Flowerpot* (2407154 points), *House* (1568490 points), *Litchi* (1039942 points), *Mushroom* (1144603 points), *Ping-pong-bat* (703879 points), *Puer-tea* (412009 points), *Pumpkin* (1340343 points), *Ship* (684617 points), *Statue* (1637577 points), *Stone* (1086453 points), and *Tool-box* (1054211 points) were chosen from the Waterloo Point Cloud (WPC) dataset [21] in the subjective evaluation. These 3DPCs have various geometric and textural complexity. Since the MPEG V-PCC platform achieves almost the best performance [6] in all the existing public encoders for both static and dynamic 3DPCs, all the 3DPCs were coded by the V-PCC test model v7 [27]. For each 3DPC, there are 25 degraded versions with five geometry QPs (26, 32, 38, 44, and 50) and five color QPs (26, 32, 38, 44, and 50). The corresponding quantization steps range from 12.75 to 204. As a result, we have $16 \times 5 \times 5 = 400$ 3DPCs in the subjective evaluation. To show a 3DPC as fully

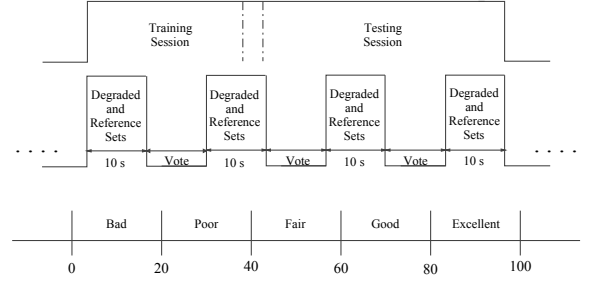


Fig. 3. Schematic diagram of the subjective experiment.



Fig. 4. Example of a subjective evaluation.

as possible, we generated 180 pictures along the horizontal and vertical directions with a step of two degrees separately, for each 3DPC, as shown in Fig. 2. Afterwards, the degraded and the original pictures were concatenated to generate a 10-second video sequence with 360 frames.

A total of 30 subjects, consisting of 15 males and 15 females aged between 20 and 35, were recruited in the subjective evaluation. All subjects had normal or corrected-to-normal vision.

B. Subjective evaluation

The Double-Stimulus Impairment Scale (DSIS) methodology [28] was adopted in the subjective evaluation. As normal operation, to expand the rating range and obtain finer distinctions, the DSIS method was adopted with 100 points continuous scale instead of 5 levels rating, as shown in Fig. 3. To display the stimuli, a DELL E2417H displayer with an In-Plane Switching Display of 23.8 inch (res. 1920 \times 1080) was used. Both the original and the distorted videos generated from a 3DPC were simultaneously shown to the observer side-by-side, as shown in Fig. 4. The observer viewed these videos from a distance equal to twice the screen height and rated them through a customized interface after the playback finished by keyboard input to guarantee there is no time restriction.

At the beginning of each evaluation, a training session was conducted to make the observers familiar with the artifacts in the assessment. The 3DPCs used for training were different from those used for the evaluation. Therefore, the observers were familiar with the distortion types and the quality levels, but not familiar with the content. The duration of each test for a given subject was about two hours, divided into four sections, with three five-minute breaks in-between to minimize the effect of fatigue.

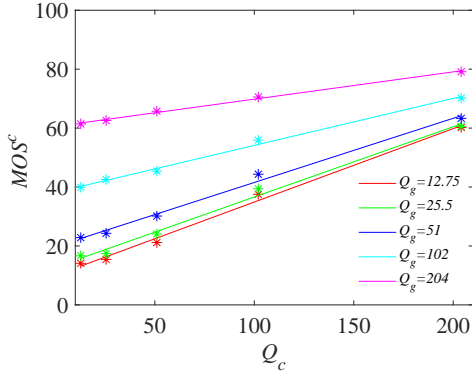


Fig. 5. Relationships between $MOS^c = 100 - MOS$ and Q_c for different Q_g s.

C. Data post-processing

Since the ratings range from 0 to 100, the scores given by different observers tend to fall in fairly small subranges. Therefore, we need to convert the subjective scores to Z-scores [29] based on the mean and standard deviation of all the scores of each observer. The Z-score of the m -th 3DPC at the j -th degraded level from the i -th viewer is

$$Z_{mij} = \frac{X_{mij} - \mu_{X_i}}{\delta_{X_i}}, \quad (1)$$

where X_{mij} denotes the raw rating, and μ_{X_i} and δ_{X_i} represent the mean and the standard deviation of the ratings of the i -th viewer, respectively. Besides, we adopted the outlier removal technique suggested in [30] to remove outliers. No participants were removed but outlier ratings from each participant were discarded. The obtained Z-scores lie in the range $[0, 100]$. The average of the Z-scores from all valid subjects were calculated to be the MOS of each degraded 3DPC. By taking the MOS as the “ground truth”, the PLCC and SRCC between each viewer’s scores and MOSs were calculated to verify the performance of individual subjects [21]. Both the mean PLCC and SRCC between each observer scores and the calculated MOS were as high as 0.84, indicating substantial agreement between individual subjects.

IV. PROPOSED QUALITY METRIC MODEL

To determine the relationship between the perceived quality and the quantization steps of the geometry and color, the distorted 3DPCs with different geometry and color quantization steps were rated, as shown in Fig. 5. We can observe that there is a linear relationship between $MOS^c = 100 - MOS$ and the the color quantization step Q_c for a fixed geometry quantization step Q_g , that is,

$$MOS^c = c_{1,g}Q_c + c_{2,g}, \quad (2)$$

where $c_{1,g}$ and $c_{2,g}$ are the model parameters. Here, we use MOS^c to represent the perceptual distortion for the standard mathematical expression used in rate-distortion optimization. From Table I, we can also see that the squared correlation coefficient (SCC) between MOS^c and Q_c with different Q_g s is larger than or equal to 0.993, while the root mean squared

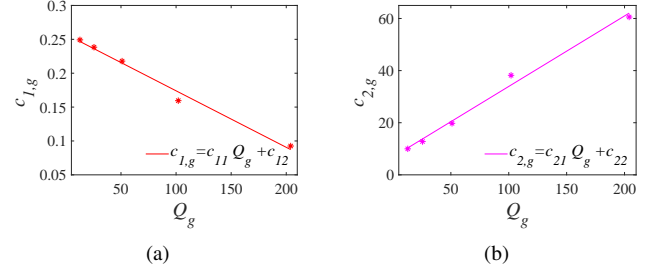


Fig. 6. Relationship between the slope $c_{1,g}$ and intercept $c_{2,g}$ in (2) and Q_g . (a) $c_{1,g}$ vs. Q_g , (b) $c_{2,g}$ vs. Q_g .

TABLE I
ACCURACY OF THE LINEAR RELATIONSHIP (2)

Q_g	$c_{1,g}$	$c_{2,g}$	SCC	RMSE
12.75	0.249	9.986	0.994	1.731
25.5	0.238	12.782	0.993	1.785
51	0.218	19.765	0.993	1.634
102	0.159	38.187	0.994	1.070
204	0.093	60.571	0.996	0.525

TABLE II
ACCURACY OF (5) FOR EACH 3DPC

Point Cloud	a	b	c	d	SCC	RMSE
<i>Bag</i>	-0.0005	0.263	0.223	3.192	0.963	4.317
<i>Banana</i>	-0.0006	0.294	0.127	19.860	0.925	5.663
<i>Biscuits</i>	-0.0006	0.190	0.204	8.293	0.964	3.158
<i>Cake</i>	-0.0008	0.303	0.188	5.519	0.977	3.192
<i>Cauliflower</i>	-0.0010	0.327	0.258	3.389	0.967	4.372
<i>Flowerpot</i>	-0.0005	0.332	0.115	13.016	0.889	8.097
<i>House</i>	-0.0012	0.311	0.361	-3.666	0.981	3.814
<i>Litchi</i>	-0.0012	0.288	0.359	-3.440	0.970	4.536
<i>Mushroom</i>	-0.0010	0.244	0.304	12.295	0.946	5.203
<i>Ping-pong_bat</i>	-0.0014	0.351	0.332	5.463	0.951	5.875
<i>Puer_tea</i>	-0.0009	0.192	0.366	6.488	0.982	3.379
<i>Pumpkin</i>	-0.0007	0.184	0.276	3.242	0.969	3.557
<i>Ship</i>	-0.0006	0.312	0.112	13.296	0.928	5.905
<i>Statue</i>	-0.0007	0.308	0.196	14.527	0.874	8.496
<i>Stone</i>	-0.0010	0.245	0.366	-1.385	0.981	3.588
<i>Tool_box</i>	-0.0008	0.184	0.333	9.886	0.951	5.124

error (RMSE) is smaller than or equal to 1.785. Moreover, as shown in Fig. 6, the relationship between the slope $c_{1,g}$ (respectively the intercept $c_{2,g}$) and Q_g can be represented by the linear models

$$c_{1,g} = c_{11}Q_g + c_{12}, \quad (3)$$

$$c_{2,g} = c_{21}Q_g + c_{22}, \quad (4)$$

where the SCCs of Q_g and $c_{1,g}$, and Q_g and $c_{2,g}$ are 0.988 and 0.990, respectively. Accordingly, the quality model can be rewritten as

$$MOS^c = aQ_gQ_c + bQ_g + cQ_c + d, \quad (5)$$

where $a = c_{11}$, $b = c_{21}$, $c = c_{12}$, and $d = c_{22}$ are model parameters. The accuracy of (5) for each 3DPC is given in Table II. By further considering the fact that the fitting parameter a is very small (Table II), (5) can be further simplified by removing the impact of $Q_g \cdot Q_c$ on the perceptual quality. This makes the model convex, which is useful in many

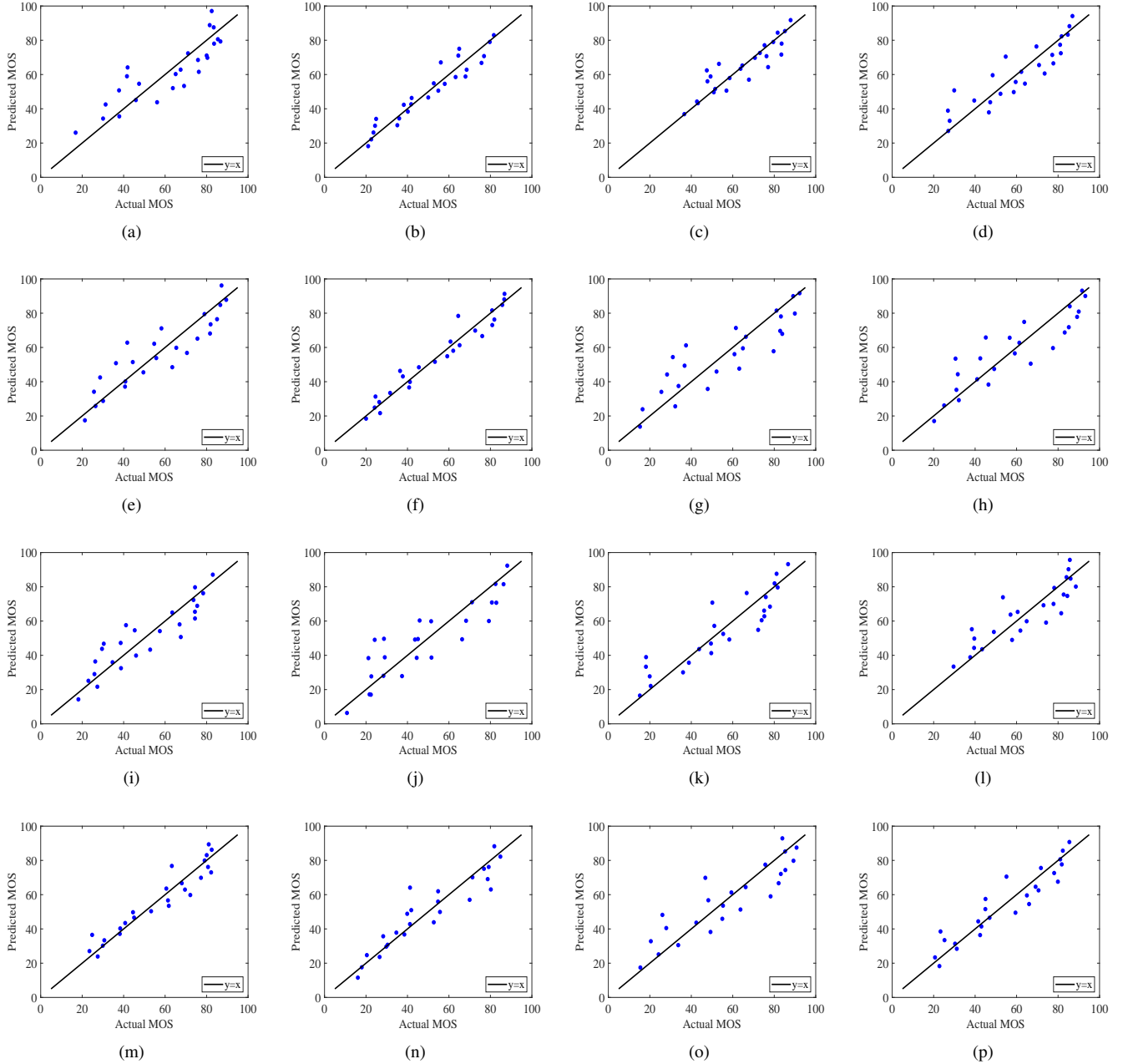


Fig. 7. Accuracy of model (5). (a)-(d): *Bag, Banana, Biscuits, and Cake*, (e)-(h): *Cauliflower, Flowerpot, House, and Litchi*, (i)-(l): *Mushroom, Ping-pong_bat, Puer_tea, and Pumpkin*, (m)-(p): *Ship, Statue, Stone, and Tool_box*.

applications such as rate-distortion optimization. Therefore, we also examined the statistical significance of the three parts in (5), i.e., $Q_g \cdot Q_c$, Q_g , and Q_c using a two-way ANOVA test [31]. In the test, the F -values are based on the ratio of mean squares (MS) of the test factor group and the error group. The MS is the mean of the square of the standard deviation (SS) that accounts for the degrees of freedom (DF). Therefore the F -value can be calculated as

$$F = MS_t / MS_e = \left(\frac{SS_t}{DF_t} \right) / \left(\frac{SS_e}{DF_e} \right) \quad (6)$$

where MS_t and MS_e represent the mean sum of squares of deviations of the test factor group and the error group, respectively. They can be calculated as $\frac{SS_t}{DF_t}$ and $\frac{SS_e}{DF_e}$, respectively, where SS_t and SS_e represent the sum of squared deviations of the test factor group and the error group, respectively, while DF_t and DF_e represent the degrees of freedom of the test factor group and the error group, respectively. Specifically, $SS_t \in \{SS_{Q_g}, SS_{Q_c}, SS_{Q_g \cdot Q_c}\}$, where $SS_{Q_g}, SS_{Q_c}, SS_{Q_g \cdot Q_c}$ denote the SS of the test factors Q_g, Q_c , and $Q_g \cdot Q_c$, respectively. Here $SS_{Q_g}, SS_{Q_c}, SS_{Q_g \cdot Q_c}$, and SS_e can be calculated as

TABLE III
TWO-WAY ANOVA ON MOS^c

Factors	Q_g	Q_c	$Q_g \cdot Q_c$
F -value	226.802	197.838	4.660

follows

$$\begin{cases} SS_{Q_g} = JL \sum_{i=1}^I (\overline{MOS_{i..}^c} - \overline{MOS^c})^2 \\ SS_{Q_c} = IL \sum_{j=1}^J (\overline{MOS_{.j}^c} - \overline{MOS^c})^2 \\ SS_{Q_g \cdot Q_c} = L \sum_{i=1}^I \sum_{j=1}^J (\overline{MOS_{ij.}^c} - \overline{MOS_{i..}^c} - \overline{MOS_{.j}^c} + \overline{MOS^c})^2 \\ SS_e = \sum_{i=1}^I \sum_{j=1}^J \sum_{l=1}^L (MOS_{ijl}^c - \overline{MOS_{ij.}^c})^2 \end{cases} \quad (7)$$

where I denotes the number of possible Q_g levels, J denotes the number of possible Q_c levels, L denotes the number of tested 3DPCs, MOS_{ijl}^c denotes the MOS^c value of the i -th Q_g level ($i = 1, 2, \dots, I$) and j -th Q_c level ($j = 1, 2, \dots, J$) for the l -th 3DPC ($l = 1, 2, \dots, L$), $\overline{MOS_{i..}^c}$ denotes the MOS^c value of the i -th Q_g level with all the possible Q_c levels for all the 3DPCs, $\overline{MOS_{.j}^c}$ denotes the MOS^c value of the j -th Q_c level with all the possible Q_g levels for all the 3DPCs, $\overline{MOS_{ij.}^c}$ denotes the MOS^c value of the i -th Q_g and the j -th Q_c level for all the 3DPCs, and $\overline{MOS^c}$ is the mean of different combinations of Q_g level, Q_c level, and the tested 3DPCs. The degree of freedom of the test factor group $DF_t \in \{DF_{Q_g}, DF_{Q_c}, DF_{Q_g \cdot Q_c}\}$ and the values of DF_{Q_g} , DF_{Q_c} , and $DF_{Q_g \cdot Q_c}$ are $I-1$, $J-1$, and $(I-1)(J-1)$, respectively. Finally, $DF_e = IJ(L-1)$. Through (6), we can calculate the corresponding F values, i.e., the MOS^c variations over $Q_g \cdot Q_c$, Q_g , and Q_c , as shown in Table III. The larger the F -value is, the more significant the corresponding parameter is. From Table III, we can see that the statistical significance of $Q_g \cdot Q_c$ is much smaller than that of Q_g and Q_c . Therefore, (5) is further simplified to

$$MOS^c = p_1 Q_g + p_2 Q_c + p_3, \quad (8)$$

where p_1 , p_2 , and p_3 are model parameters. By using (8), the SCC between the fitted MOS^c and the actual one is up to 0.949. The model parameters p_1 , p_2 , and p_3 in (8), the SCCs, and the RMSEs between the actual MOS^c s and the fitted values of all the evaluated 3DPCs are given in Table IV. We can see that the average SCC is 0.914, indicating that the derived simplified perceptual quality model is accurate. Fig. 7 illustrates the accuracy of (8).

V. MODEL PARAMETER PREDICTION USING CONTENT FEATURES

As shown in Fig. 8, 3DPCs with rich texture characteristics (e.g., *Cake*) usually have lower MOS^c (corresponding to higher MOS) for the same quantization steps. In contrast, 3DPCs with simple texture characteristics (e.g., *Ping-pong_bat*) have higher MOS^c (corresponding to lower MOS) for the same quantization steps. This is because the content has a concealing effect on the coding distortion, which is consistent with the characteristics of the human visual system [32]. That is to say, the model parameters are highly content dependent. In this section, we propose two features to predict the model parameters efficiently. The perceptual

TABLE IV
PARAMETERS AND ACCURACY OF THE PERCEPTUAL QUALITY MODEL

Point Cloud	p_1	p_2	p_3	SCC	RMSE
<i>Bag</i>	0.223	0.183	6.342	0.949	4.954
<i>Banana</i>	0.247	0.080	23.601	0.902	6.336
<i>Biscuits</i>	0.143	0.156	12.072	0.927	4.387
<i>Cake</i>	0.241	0.125	10.489	0.938	5.153
<i>Cauliflower</i>	0.246	0.177	9.773	0.916	6.782
<i>Flowerpot</i>	0.291	0.075	16.212	0.877	8.339
<i>House</i>	0.220	0.269	3.597	0.930	7.059
<i>Litchi</i>	0.195	0.266	3.874	0.914	7.488
<i>Mushroom</i>	0.164	0.225	18.579	0.890	7.262
<i>Ping-pong_bat</i>	0.240	0.221	14.240	0.872	9.243
<i>Puer_tea</i>	0.124	0.297	11.921	0.948	5.568
<i>Pumpkin</i>	0.131	0.223	7.424	0.939	4.898
<i>Ship</i>	0.268	0.068	16.756	0.910	6.438
<i>Statue</i>	0.254	0.142	18.777	0.852	9.011
<i>Stone</i>	0.170	0.291	4.555	0.945	6.026
<i>Tool_box</i>	0.117	0.266	15.152	0.914	6.630
Average	-	-	-	0.914	6.598

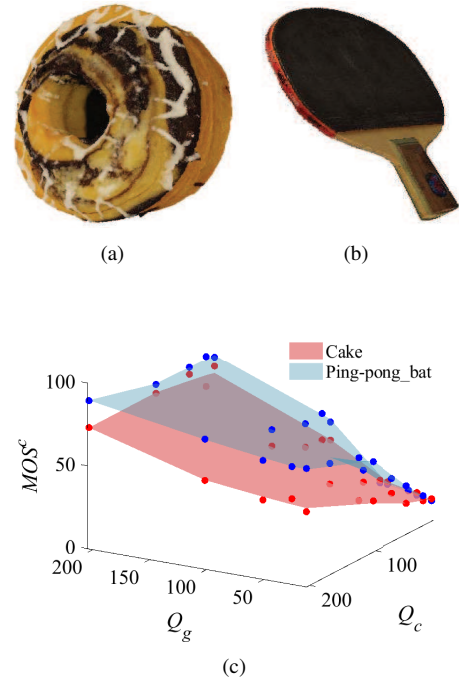


Fig. 8. Relationship between content complexity and MOS^c . (a) *Cake*, (b) *Ping-pong_bat*, (c) mesh curve of MOS^c , Q_g , and Q_c for *Cake* and *Ping-pong_bat*.

quality of a 3DPC depends on both the geometry and color distortion. But the influence of geometry and color distortion are different [33]. By analyzing the local topological and color consistencies, Alexiou and Ebrahimi [34] and Meynet *et al.* [35] reported that color-based features achieve the best performance in predicting the perceptual quality. Accordingly, we extracted two novel texture features (a local feature and a global feature) to predict the model parameters effectively. The local feature represents the color fluctuation over a geometric distance (CFGD), while the global feature is the color block mean variance (CBMV).

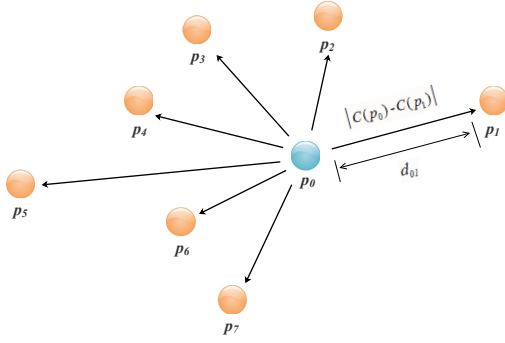


Fig. 9. Illustration of the calculation of CFGD.

A. Color fluctuation over geometric distance (CFGD)

Color gradient appropriately describes local texture variation, therefore, we define the CFGD to describe the local content characteristic for a 3DPC. As shown in Fig. 9, the mean value of the neighboring color intensity differences of the current point is calculated to be the CFGD feature of the point:

$$CFGD_i = \frac{1}{N_i} \sum_{p_j \in S_i} \frac{|C(p_i) - C(p_j)|}{d_{i,j}}, \quad (9)$$

where $CFGD_i$ denotes the value of CFGD for point p_i , $C(\cdot)$ denotes the color attribute of a point, $d_{i,j}$ denotes the distance between points p_i and p_j , S_i is the set of the K nearest neighbors of point p_i , and N_i is the number of points in S_i . For simplicity, we only consider the Y (luminance) component [36] in this paper. Then, the CFGD of all the points is defined as

$$CFGD = \frac{1}{T} \sum_{i \in \mathbb{P}} CFGD_i, \quad (10)$$

where T is the number of points in the 3DPC \mathbb{P} .

B. Color block mean variance (CBMV)

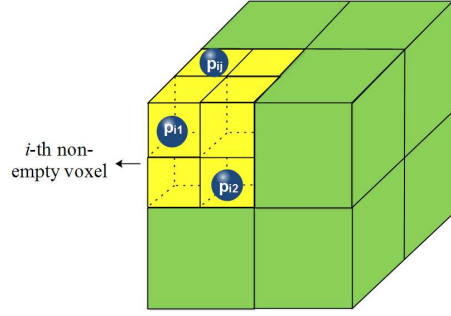
The standard deviation is commonly used as a global feature for image/video quality assessment [37] [38] [39]. Similarly, we use it to build a global feature for 3DPCs. Assuming that the 3DPCs are voxelized [40] (Fig. 10), the CBMV is computed as

$$CBMV = \frac{1}{B} \sum_{i=1}^B \sqrt{\frac{1}{D} \sum_{j=1}^D (C(p_{ij}) - \mu_i)^2}, \quad (11)$$

where B denotes the number of non-empty voxels, D denotes the number of points in the i -th non-empty voxel, $C(p_{ij})$ is the color of the j -th point in the i -th non-empty voxel, and μ_i is the color mean value of the i -th non-empty voxel.

C. Model parameter estimation

We used a generalized linear model (GLM) [41] to predict the model parameters from the extracted two features. Let $p_{m,j}$ denote the j -th parameter in (8) of the m -th 3DPC, $m = 1, 2, \dots, M$, where M is the number of 3DPCs. Let $f_{m,k}$ denotes the value of the k -th feature for the m -th 3DPC,

Fig. 10. Voxelized 3DPC. The voxel size can be 8^3 , 16^3 , 32^3 , or 64^3

$k = 1, 2, \dots, K$, and K is the number of extracted features (in this paper, $K = 2$). Then, the parameter $p_{m,j}$ is estimated by a generalized linear predictor

$$p_{m,j} = h_{j,0} + \sum_{k=1}^K f_{m,k} h_{j,k}, \quad (12)$$

where $h_{j,k}$ is the weight of the j -th parameter in (8) of the k -th feature, $j = 1, 2$, and 3. The $h_{j,0}$ is the constant weight of the j -th parameter. The generalized linear predictor can be described using the vector form $\hat{\mathbf{P}}_m = \mathbf{F}_m \mathbf{H}$, where $\hat{\mathbf{P}}_m$ is a three-dimensional vector, representing the model parameters $[p_1, p_2, p_3]$ in (8) of the m -th 3DPC, and $\mathbf{F}_m = [1, f_{m,1}, f_{m,2}]$, where $f_{m,1}$ and $f_{m,2}$ represent the two feature values of the m -th 3DPC. \mathbf{H} is a $3 \times (K + 1)$ coefficients matrix with elements $h_{j,k}$. The aim is to find a matrix \mathbf{H} that minimizes the prediction error ε .

In this paper, \mathbf{H} is obtained by training, and we set the voxel size equal to 64^3 as an example for the CBMV. Eight 3DPCs: *Cauliflower*, *Stone*, *House*, *Ship*, *Tool_box*, *Pumpkin*, *Biscuits* and *Ping-pong_bat* that cover a wide range of content characteristics were used for training. The remaining 3DPCs, i.e., *Litchi*, *Puer_tea*, *Flowerpot*, *Bag*, *Cake*, *Statue*, *Banana* and *Mushroom* were used for testing. We determined the optimal \mathbf{H} by minimizing the fitting error ε for the training 3DPCs set, defined as

$$\varepsilon = \sum_{m=1}^8 \|\hat{\mathbf{P}}_m - \mathbf{P}_m\|^2. \quad (13)$$

where $\hat{\mathbf{P}}_m$ and \mathbf{P}_m are the predicted model parameter vector and the model parameter vector of the m -th 3DPC, respectively. The optimal \mathbf{H} is then calculated to be

$$\mathbf{H}^{\text{opt}} = \begin{bmatrix} 0.1817 & 0.2058 & 18.4528 \\ 0.0034 & -0.0070 & -0.0199 \\ -0.0116 & 0.0292 & -1.5427 \end{bmatrix}. \quad (14)$$

By using \mathbf{H}^{opt} and the extracted feature vector \mathbf{F}_m , the model parameter vector $\hat{\mathbf{P}}_m$ can be calculated directly. Furthermore, based on the estimated model parameters, we can obtain the MOS^c through (8). We use PLCC, SRCC [42], and RMSE between the actual MOS^c s and the predicted ones to evaluate the accuracy of the proposed model with the estimated parameters. Table V shows that the PLCC and

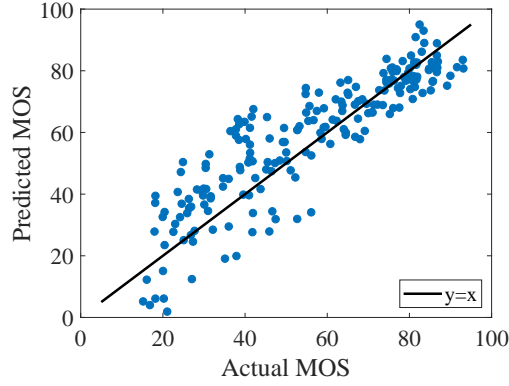


Fig. 11. Scatter plot of the actual MOS and the MOS predicted by the proposed quality model for the test set.

TABLE V
PERFORMANCE OF THE PERCEPTUAL QUALITY MODEL ON THE TRAINING AND TEST SETS. V_{size} IS THE VOXEL SIZE FOR CBMV

DataSet	V_{size}	PLCC	SRCC	RMSE
Training Set	8^3	0.9291	0.9358	8.1530
	16^3	0.9335	0.9377	7.9047
	32^3	0.9369	0.9402	7.7078
	64^3	0.9377	0.9409	7.6597
Test Set	8^3	0.8963	0.8922	9.7016
	16^3	0.8998	0.8972	9.5457
	32^3	0.9080	0.9053	9.1651
	64^3	0.9133	0.9095	8.9090

SRCC of the proposed perceptual quality model of the test set are as high as 0.9133 and 0.9095, respectively, and RMSE is as small as 8.9090 (noting that the maximum MOS is 100). The accuracy of the model is also illustrated in Fig. 11 which shows the relationship between the actual MOSs and the estimated ones. To further validate the accuracy of the proposed RR quality metric model, we compared it to three the representative FR objective metric models: a point-based model [9], a projection-based model [20] [43] [44] [45], and a graph-based model [23]. The point-based method captures the difference between the points in the reference and the tested 3DPC, and we name it as $PSNR_Y$. Currently, the point-based method is adopted by MPEG. For the projection-based approaches, a 3DPC is mapped onto six conventional two-dimensional image planes by orthographic projection. After obtaining the projected image planes, the 2D image quality metrics structural similarity (SSIM) [44], multi-scale structural similarity (MS-SSIM) [45], and visual information fidelity in pixel domain (VIFP) [43] are used to evaluate the six projection image quality, finally, the average image quality of these six projection is mapped to MOS by the best fitting logistic function, the mapped MOS is taken as the quality of the 3DPC. We call these projection-based methods $SSIM_{projection}$, $MS-SSIM_{projection}$, and $VIFP_{projection}$, respectively. For the graph-based method [23], local graphs centered at the key points were used to calculate the similarity between the original and the distorted 3DPC. We call this method GraphSIM. Table VI shows the comparison results

TABLE VI
PERFORMANCE OF POINT CLOUD QUALITY ASSESSMENT MODELS.

Model Type	Model	PLCC	SRCC	RMSE
FR	$PSNR_Y$	0.3956	0.3926	20.2058
	$SSIM_{projection}$	0.4027	0.4014	20.1382
	$MS-SSIM_{projection}$	0.5126	0.5025	18.8910
	$VIFP_{projection}$	0.8199	0.8187	12.5964
	GraphSIM	0.7748	0.7786	13.9095
RR	proposed ($V_{size} = 64^3$)	0.9133	0.9095	8.9090

with the point-based and projection-based methods. We can see that the point-based $PSNR_Y$ model does not seem to provide enough accuracy due to a lack of overall perception. GraphSIM improves the prediction accuracy to some extent; however, it is more complex and requires many parameters to be determined. In contrast, the projection-based models perform better among which VIFP achieves the best performance compared to PSNR, SSIM and MS-SSIM. Nevertheless, the quality prediction accuracy is only moderate when compared with their performance on 2D images [21]. Table VI shows that the PLCC of FR quality metrics is in the range 0.4027 to 0.8199. In contrast, the PLCC of the proposed RR quality metric is as high as 0.9133. In addition to the PLCC, the SRCC of the worst and best FR quality metrics are 0.3926 and 0.8187 respectively, whereas the SRCC of the proposed RR quality metric is 0.9095. Beyond that, the RMSE of the proposed quality metric is also much smaller than those compared metrics. Fig. 12 shows scatter plots of MOS vs. objective scores for all models. The plots illustrate the superiority of the proposed RR quality metric over the other models.

VI. APPLICATION

The developed perceptual quality model would be of great benefit to applications involving coding and rate control in 3DPC broadcasting systems. In this paper, we solve the rate control problem for a static 3DPC. Our method can also be extended to dynamic 3DPCs as they can be seen as a sequence of successive static 3DPCs. For a given target bitrate, we aim to find the combination of the geometry QP (corresponding to Q_g) and color QP (corresponding to Q_c) that provide the best perceptual quality. We formulate this rate control problem as a constrained optimization problem where the objective function is the derived perceptual quality model,

$$\begin{aligned} \min_{(Q_g, Q_c)} \quad & MOS^c(Q_g, Q_c) \\ \text{s.t.} \quad & R_g(Q_g) + R_c(Q_g, Q_c) \leq R_T, \end{aligned} \quad (15)$$

where R_g and R_c are the geometry and color bitrate, respectively, and R_T is the overall target bitrate. Based on (8), (15) and the Cauchy-based rate model [25], the rate control problem can be rewritten as

$$\begin{aligned} \min_{(Q_g, Q_c)} \quad & p_1 Q_g + p_2 Q_c + p_3 \\ \text{s.t.} \quad & \gamma_g Q_g^{\theta_g} + \gamma_c Q_c^{\theta_c} \leq R_T, \end{aligned} \quad (16)$$

where p_1 , p_2 , and p_3 are the parameters of the perceptual quality model, and γ_g , θ_g , γ_c , θ_c are the parameters of the geometry and color rate models.

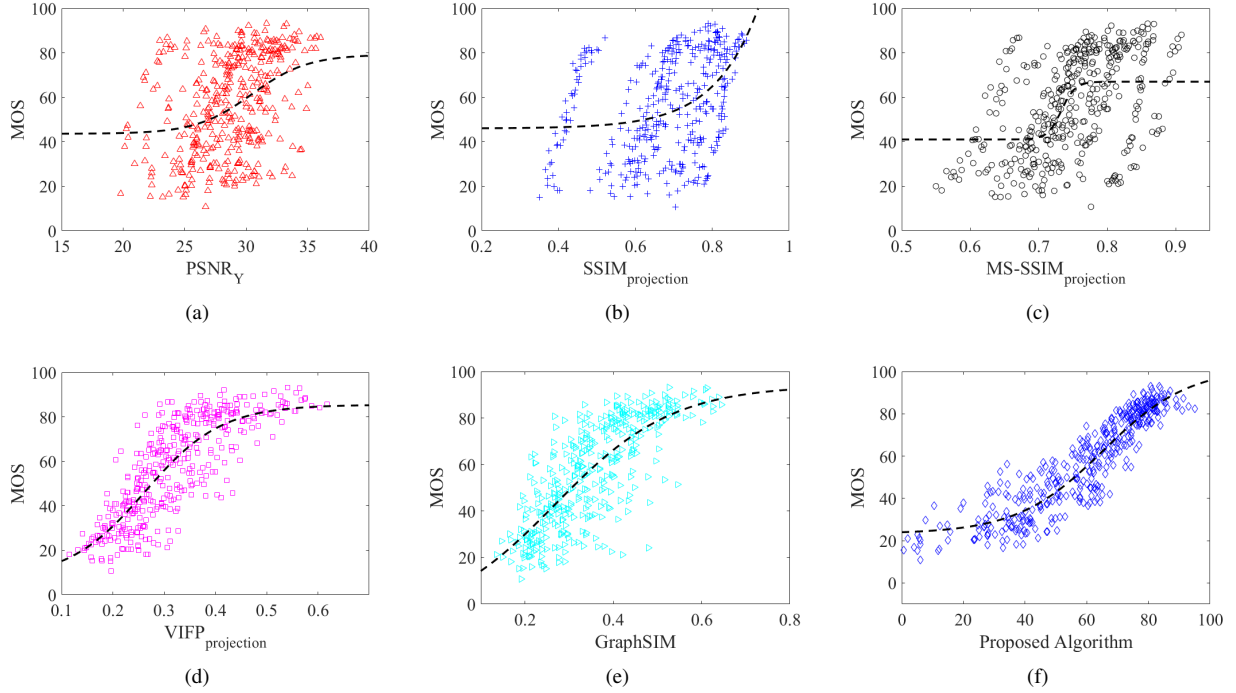


Fig. 12. Scatter plots of objective score vs. MOS. The dashed curves correspond to the best fitting logistic functions.

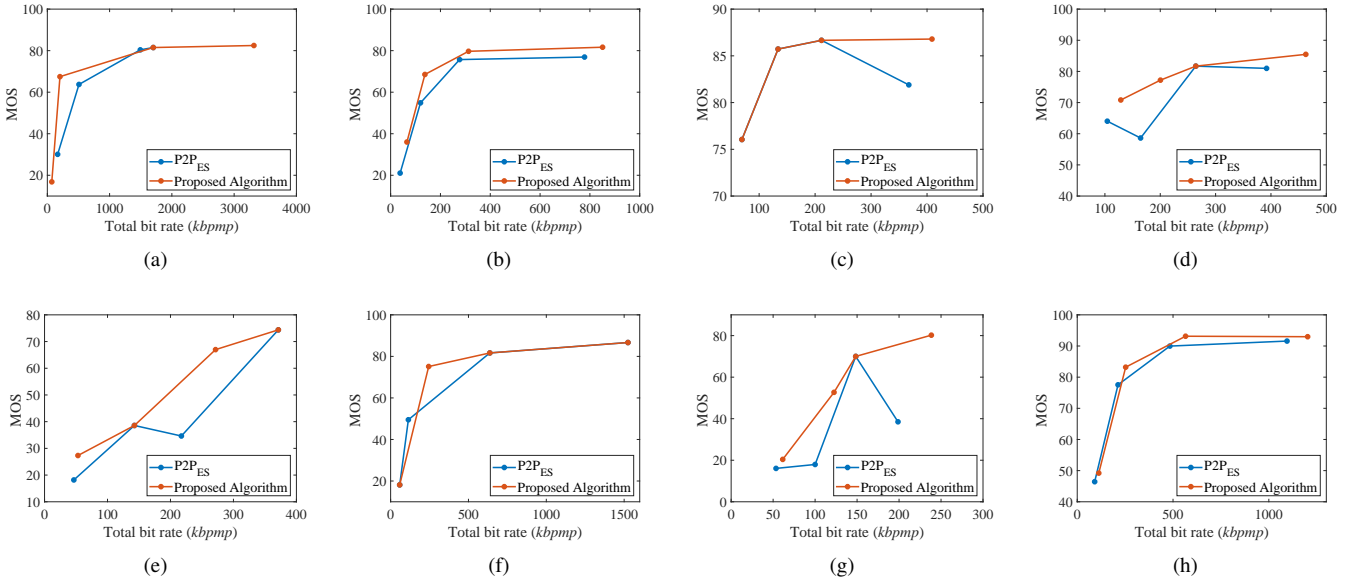


Fig. 13. MOS vs. total bit rate for our rate control algorithm and the point-to-point exhaustive search algorithm ($P2P_{ES}$). (a) *Bag*, (b) *Banana*, (c) *Flowerpot*, (d) *Cake*, (e) *Mushroom*, (f) *Puer_tea*, (g) *Statue*, (h) *Litchi*. The vertical axis shows the average MOS of all the viewers.

Together with the proposed model parameter estimation method in Section V, the proposed model can be embedded in the V-PCC (TMC2) encoder to determine the optimal Q_g and Q_c . First, the CFGD and CBMV features of the input 3DPC are extracted, as described in Section V. Then by using the pre-trained matrix \mathbf{H} in (14), the parameter vector $\hat{\mathbf{P}}_m$ can be calculated. For the rate model, the parameters γ_g , θ_g , γ_c , and θ_c can be obtained by precoding with two geometry and color quantization step pairs. Finally, with the target bitrate R_T , the optimal $Q_{g,opt}$ and $Q_{c,opt}$ can be obtained by solving (16)

using an interior point method or another convex optimization method [46].

To assess the proposed perceptual quality model-based rate control algorithm, we compared its performance to that of point-to-point based exhaustive search algorithm (denoted by $P2P_{ES}$). For $P2P_{ES}$, a 3DPC was first encoded by all the tested geometry and color QP pairs ranging from 26 to 50. Then the subset of admissible pairs (pairs whose bitrates are smaller than or equal to the target bitrate) was determined. Finally, the pair that gave the highest PSNR for

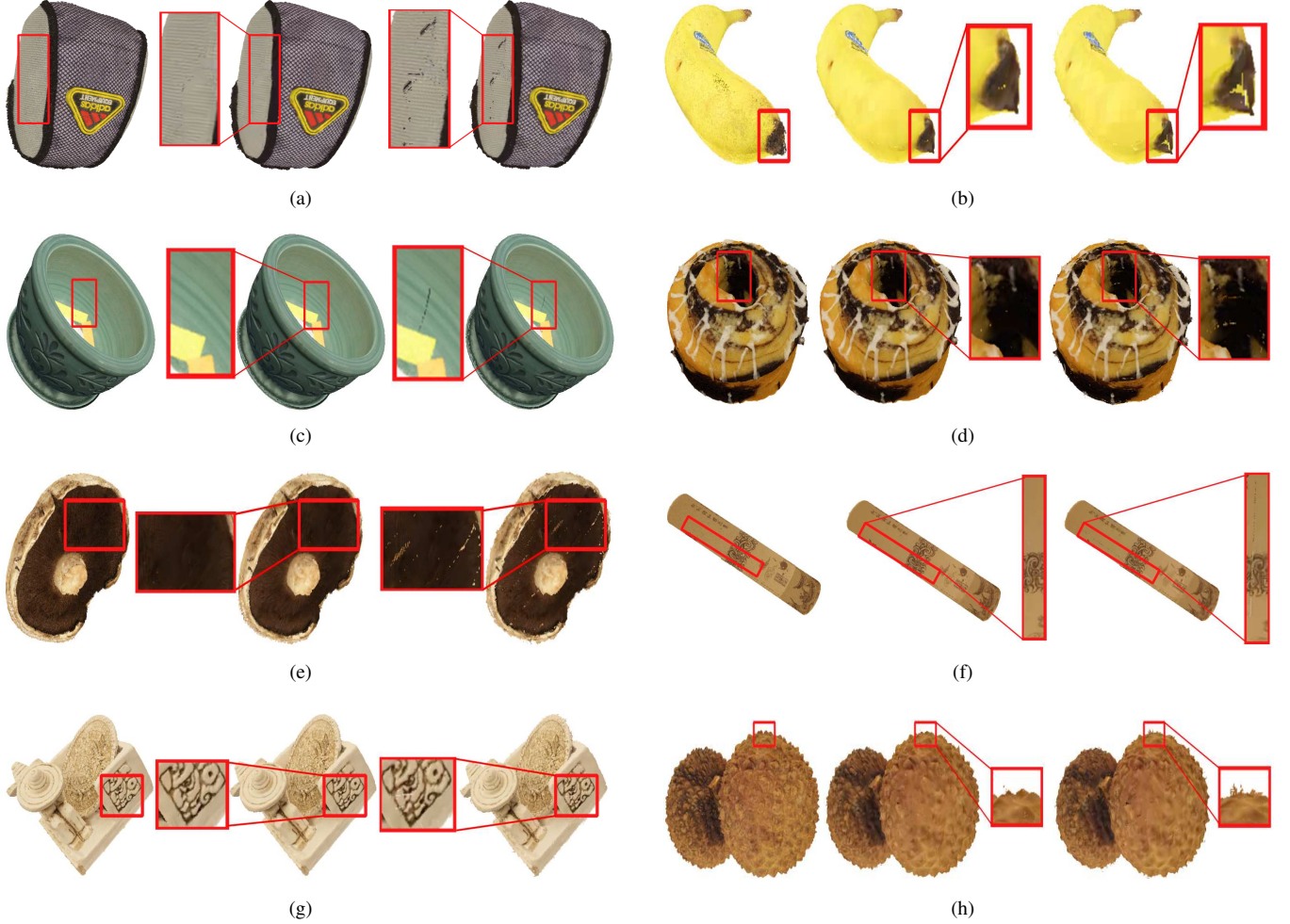


Fig. 14. Perceptual quality comparison between our rate control algorithm and $P2PES$. Left: original, Centre: proposed, Right: $P2PES$. (a) subjective quality of *Bag* with a target bitrate of 510 kbpmp, (b) subjective quality of *Banana* with a target bitrate of 85 kbpmp, (c) subjective quality of *Flowerpot* with a target bitrate of 405 kbpmp, (d) subjective quality of *Cake* with a target bitrate of 170 kbpmp, (e) subjective quality of *Mushroom* with a target bitrate of 275 kbpmp, (f) subjective quality of *Puer_tea* with a target bitrate of 190 kbpmp, (g) subjective quality of *Statue* with a target bitrate of 165 kbpmp, (h) subjective quality of *Litchi* with a target bitrate of 110 kbpmp.

TABLE VII
TARGET BITRATE IN KILOBITS PER MILLION POINTS (kbpmp) FOR EACH
POINT CLOUD IN THE TEST SET

Point Cloud	$R_{T,1}$	$R_{T,2}$	$R_{T,3}$	$R_{T,4}$
<i>Bag</i>	170	510	1495	2130
<i>Banana</i>	40	120	310	850
<i>Cake</i>	110	170	265	460
<i>Flowerpot</i>	75	135	265	405
<i>Litchi</i>	110	250	565	1200
<i>Mushroom</i>	50	150	220	375
<i>Puer_tea</i>	75	190	640	1525
<i>Statue</i>	55	105	155	200

the Y component ($PSNR_Y$) was selected from this subset. We focused on the Y component because it plays an important role in visualization and in our perception of objective structure and surface shape [47]. Since the texture complexity of the tested 3DPCs are different, we set different target bitrates for each 3DPC, as shown in Table VII. The rate-MOS curves of the proposed algorithm and $P2PES$ are compared in Fig. 13. The results demonstrate that the proposed rate

control algorithm can achieve better rate-MOS performance than $P2PES$ with much lower complexity. Since the value of $PSNR_Y$ in $P2PES$ is not consistent with the MOS , the MOS s of the reconstructed 3DPCs by the $P2PES$ fluctuate with different target bitrates. The proposed algorithm used the proposed RR model to better predict the MOS s, and better subjective quality can be achieved with given target bitrates. Finally, Fig. 14 compares the subjective quality between the proposed rate control algorithm and $P2PES$. We can see that a significant subjective quality improvement can be achieved by the proposed RR model-based rate control algorithm.

VII. CONCLUSION

We proposed an RR linear quality model that accurately predicts the perceptual quality of V-PCC compressed 3DPCs from the V-PCC geometry and color quantization parameters. The three coefficients of our linear model are estimated using a training set of reference 3DPCs and two features (CFGD and CBMV) that are computed from the test reference 3DPC. Because the number of high quality original 3DPCs used by

the MPEG PCC group is rather limited, we selected high quality 3DPCs from the WPC dataset to conduct the subjective experiments for static 3DPCs. The results show that the PLCC and the SRCC between the predicted MOSs and the actual MOSs are both as high as 0.91, indicating high accuracy of the proposed model.

Moreover, to illustrate the applications of the proposed model, we also proposed an optimized rate control algorithm for 3DPC compression. Benefitting from the accuracy of the proposed RR quality model, the subjective quality of the proposed algorithm is much better than that of $P2P_{ES}$.

In future work, we will assess the performance of the proposed model on the high quality 3DPCs recently provided by the MPEG PCC group. We will also apply the proposed quality metric to rate-distortion optimized coding and quality enhancement for 3DPCs.

REFERENCES

- [1] S. Gu, J. Hou, H. Zeng, H. Yuan, and K.-K. Ma, "3D point cloud attribute compression using geometry-guided sparse representation," *IEEE Transactions on Image Processing*, vol. 29, pp. 796–808, 2019.
- [2] L. Li, Z. Li, V. Zakharchenko, J. Chen, and H. Li, "Advanced 3D motion prediction for video-based dynamic point cloud compression," *IEEE Transactions on Image Processing*, vol. 29, pp. 289–302, 2020.
- [3] S. Gu, J. Hou, H. Zeng, and H. Yuan, "3D point cloud attribute compression via graph prediction," *IEEE Signal Processing Letters*, vol. 27, pp. 176–180, 2020.
- [4] 3DG, "Text of ISO/IEC CD 23090-9 geometry-based point cloud compression," *Doc. ISO/IEC JTC1/SC29/WG11 MPEG N18478*, Geneva, Switzerland, Mar. 2019.
- [5] —, "Text of ISO/IEC CD 23090-5: Video-based point cloud compression," *ISO/IEC JTC1/SC29/WG11 MPEG N18030*, Macau, China, Oct. 2018.
- [6] H. Liu, H. Yuan, Q. Liu, J. Hou, and J. Liu, "A comprehensive study and comparison of core technologies for mpeg 3-D point cloud compression," *IEEE Transactions on Broadcasting*, vol. 66, no. 3, pp. 701–717, Dec. 2020.
- [7] D. Girardeau-Montaut, M. Roux, R. Marc, and G. Thibault, "Change detection on points cloud data acquired with a ground laser scanner," *International Archives of Photogrammetry, Remote Sensing and Spatial Information Sciences*, vol. 36, p. W19, 2005.
- [8] D. Tian, H. Ochimizu, C. Feng, R. Cohen, and A. Vetro, "Geometric distortion metrics for point cloud compression," in *2017 IEEE International Conference on Image Processing (ICIP)*. IEEE, 2017, pp. 3460–3464.
- [9] R. Mekuria, Z. Li, C. Tulvan, and P. Chou, "Evaluation criteria for PCC (point cloud compression)," *ISO/IEC JTC1/SC29/WG11 MPEG N16332*, 2016.
- [10] E. Alexiou and T. Ebrahimi, "Point cloud quality assessment metric based on angular similarity," in *2018 IEEE International Conference on Multimedia and Expo (ICME)*. IEEE, 2018, pp. 1–6.
- [11] G. Meynet, J. Digne, and G. Lavoué, "PC-MSDM: A quality metric for 3D point clouds," in *2019 Eleventh International Conference on Quality of Multimedia Experience (QoMEX)*. IEEE, 2019, pp. 1–3.
- [12] E. Alexiou and T. Ebrahimi, "On subjective and objective quality evaluation of point cloud geometry," in *2017 Ninth International Conference on Quality of Multimedia Experience (QoMEX)*. IEEE, 2017, pp. 1–3.
- [13] E. Alexiou, T. Ebrahimi, M. V. Bernardo, M. Pereira, A. Pinheiro, L. A. D. S. Cruz, C. Duarte, L. G. Dmitrovic, E. Dumic, D. Matkovic *et al.*, "Point cloud subjective evaluation methodology based on 2D rendering," in *2018 Tenth International Conference on Quality of Multimedia Experience (QoMEX)*. IEEE, 2018, pp. 1–6.
- [14] E. Alexiou, I. Viola, T. M. Borges, T. A. Fonseca, R. L. de Queiroz, and T. Ebrahimi, "A comprehensive study of the rate-distortion performance in MPEG point cloud compression," *APSIPA Transactions on Signal and Information Processing*, vol. 8, 2019.
- [15] E. Zerman, P. Gao, C. Ozcinar, and A. Smolic, "Subjective and objective quality assessment for volumetric video compression," *Electronic Imaging*, vol. 2019, no. 10, pp. 323–1, 2019.
- [16] E. Alexiou and T. Ebrahimi, "Impact of visualisation strategy for subjective quality assessment of point clouds," in *2018 IEEE International Conference on Multimedia & Expo Workshops (ICMEW)*. IEEE, 2018, pp. 1–6.
- [17] Point cloud subjective assessment database. [Online]. Available: <https://vision.nju.edu.cn/28/fd/c29466a469245/page.htm>
- [18] A. Javaheri, C. Brites, F. Pereira, and J. Ascenso, "Subjective and objective quality evaluation of compressed point clouds," in *2017 IEEE 19th International Workshop on Multimedia Signal Processing (MMSp)*, Oct 2017, pp. 1–6.
- [19] E. Alexiou and T. Ebrahimi, "On the performance of metrics to predict quality in point cloud representations," in *Applications of Digital Image Processing XL*, vol. 10396. International Society for Optics and Photonics, 2017.
- [20] E. M. Torlig, E. Alexiou, T. A. Fonseca, R. L. de Queiroz, and T. Ebrahimi, "A novel methodology for quality assessment of voxelized point clouds," in *Applications of Digital Image Processing XLI*, vol. 10752. International Society for Optics and Photonics, 2018.
- [21] H. Su, Z. Duanmu, W. Liu, Q. Liu, and Z. Wang, "Perceptual quality assessment of 3D point clouds," in *2019 IEEE International Conference on Image Processing (ICIP)*. IEEE, 2019, pp. 3182–3186.
- [22] L. N. Thibos, "Image processing by the human eye," in *Visual Communications and Image Processing IV*, vol. 1199. International Society for Optics and Photonics, 1989, pp. 1148–1153.
- [23] Q. Yang, Z. Ma, Y. Xu, Z. Li, and J. Sun, "Inferring point cloud quality via graph similarity," *arXiv preprint arXiv:2006.00497*, 2020.
- [24] Q. Liu, H. Yuan, J. Hou, H. Liu, and R. Hamzaoui, "Model-based encoding parameter optimization for 3D point cloud compression," in *2018 Asia-Pacific Signal and Information Processing Association Annual Summit and Conference (APSIPA ASC)*. IEEE, 2018, pp. 1981–1986.
- [25] Q. Liu, H. Yuan, J. Hou, R. Hamzaoui, and H. Su, "Model-based joint bit allocation between geometry and color for video-based 3D point cloud compression," *IEEE Transactions on Multimedia*, 2020 DOI:10.1109/TMM.2020.3023294.
- [26] Q. Liu, H. Yuan, R. Hamzaoui, and H. Su, "Coarse to fine rate control for region-based 3D point cloud compression," in *2020 IEEE International Conference on Multimedia & Expo Workshops (ICMEW)*. IEEE, 2020, pp. 1–6.
- [27] MPEG 3DG. (2019) V-PCC test model v7. [Online]. Available: <http://mpegx.int-evry.fr/software/MPEG/PCC/TM/mpeg-pcc-tmc2.git>
- [28] Y. Nehmé, J.-P. Farrugia, F. Dupont, P. LeCallet, and G. Lavoué, "Comparison of subjective methods, with and without explicit reference, for quality assessment of 3D graphics," in *ACM Symposium on Applied Perception 2019*, 2019, pp. 1–9.
- [29] A. M. Van Dijk, J.-B. Martens, and A. B. Watson, "Quality assessment of coded images using numerical category scaling," in *Advanced Image and Video Communications and Storage Technologies*, vol. 2451. International Society for Optics and Photonics, 1995, pp. 90–101.
- [30] ITU, "Methodology for the subjective assessment of the quality of television pictures," *Recommendation BT.500-13*, 2012.
- [31] E. R. Girden, *ANOVA: Repeated measures*. Sage Publications, Inc, 1992.
- [32] S. A. Karunasekera and N. G. Kingsbury, "A distortion measure for blocking artifacts in images based on human visual sensitivity," *IEEE Transactions on image processing*, vol. 4, no. 6, pp. 713–724, 1995.
- [33] A. Javaheri, C. Brites, F. Pereira, and J. Ascenso, "Point cloud rendering after coding: Impacts on subjective and objective quality," *arXiv preprint arXiv:1912.09137*, 2019.
- [34] E. Alexiou and T. Ebrahimi, "Towards a point cloud structural similarity metric," in *2020 IEEE International Conference on Multimedia and Expo Workshops (ICMEW)*, 2020.
- [35] G. Meynet, Y. Nehmé, J. Digne, and G. Lavoué, "PCQM: A full-reference quality metric for colored 3D point clouds," in *12th International Conference on Quality of Multimedia Experience (QoMEX 2020)*, 2020.
- [36] R. Mekuria, S. Laserra, and C. Tulvan, "Performance assessment of point cloud compression," in *2017 IEEE Visual Communications and Image Processing (VCIP)*. IEEE, 2017, pp. 1–4.
- [37] Y. Fang, K. Ma, Z. Wang, W. Lin, Z. Fang, and G. Zhai, "No-reference quality assessment of contrast-distorted images based on natural scene statistics," *IEEE Signal Processing Letters*, vol. 22, no. 7, pp. 838–842, 2014.
- [38] S. Rimac-Drlje, D. Zagar, and G. Martinovic, "Spatial masking and perceived video quality in multimedia applications," in *2009 16th International Conference on Systems, Signals and Image Processing*. IEEE, 2009, pp. 1–4.

- [39] W. Xue, L. Zhang, X. Mou, and A. C. Bovik, "Gradient magnitude similarity deviation: A highly efficient perceptual image quality index," *IEEE Transactions on Image Processing*, vol. 23, no. 2, pp. 684–695, 2013.
- [40] D. Thanou, P. A. Chou, and P. Frossard, "Graph-based compression of dynamic 3D point cloud sequences," *IEEE Transactions on Image Processing*, vol. 25, no. 4, pp. 1765–1778, 2016.
- [41] A. J. Dobson and A. G. Barnett, *An introduction to generalized linear models*. CRC press, 2018.
- [42] J. Antkowiak, T. Jamal Baina, F. V. Baroncini, N. Chateau, F. FranceT-elecom, A. C. F. Pessoa, F. Stephanie Colonnese, I. L. Contin, J. Caviedes, and F. Philips, "Final report from the video quality experts group on the validation of objective models of video quality assessment march 2000," 2000.
- [43] H. R. Sheikh and A. C. Bovik, "Image information and visual quality," *IEEE Transactions on image processing*, vol. 15, no. 2, pp. 430–444, 2006.
- [44] Z. Wang, A. C. Bovik, H. R. Sheikh, and E. P. Simoncelli, "Image quality assessment: from error visibility to structural similarity," *IEEE Transactions on Image Processing*, vol. 13, no. 4, pp. 600–612, 2004.
- [45] Z. Wang, E. P. Simoncelli, and A. C. Bovik, "Multiscale structural similarity for image quality assessment," in *The Thirty-Seventh Asilomar Conference on Signals, Systems & Computers, 2003*, vol. 2. IEEE, 2003, pp. 1398–1402.
- [46] S. Boyd and L. Vandenberghe, *Convex optimization*. Cambridge University press, 2004.
- [47] S. E. Palmer, *Vision science: Photons to phenomenology*. MIT press, 1999.